Fusion Engineering and Design 202 (2024) 114335

Contents lists available at ScienceDirect

Fusion Engineering and Design

journal homepage: www.elsevier.com/locate/fusengdes

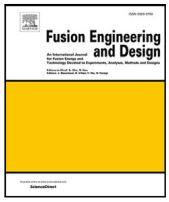

Thermofluid-dynamic and thermal–structural assessment of the EU-DEMO WCLL "double bundle" Breeding Blanket concept left outboard segment

P.A. Di Maio [a,*], I. Catanzaro [a], G. Bongiovì [a], F.M. Castrovinci [a], P. Chiovaro [a], S. Giambrone [a], A. Gioè [a], F.A. Hernández [b], I. Moscato [b], G.A. Spagnuolo [b], A. Quartararo [a], E. Vallone [a]

[a] Department of Engineering, University of Palermo, Viale delle Scienze Ed. 6, 90128, Palermo, Italy
[b] Fusion Technology Department – Programme Management Unit, EUROfusion Consortium, Boltzmannstraße 2, 85748, Garching, Germany

ARTICLE INFO

Keywords:
DEMO
Breeding Blanket
WCLL
Thermofluid-dynamics
CFD analysis
FEM analysis

ABSTRACT

As part of the activities performed by the DEMO Central Team (DCT) to study alternative configurations of the Water-Cooled Lead Lithium (WCLL) Breeding Blanket (BB), to overcome the open issues that emerged at the end of the Pre-Conceptual Design phase, a new concept, the WCLL BB "double bundle" (db), was developed. This concept adopts an array of db tubes poloidally distributed inside the breeding zone, mimicking the arrangement inside heat exchangers. These are coaxial pipes the gap between which is filled with PbBi (or alternatively with gas and fins), which avoids direct contact between PbLi and water in case of in-box LOCA events. Similarly, the First Wall channel cooling water is separated from the PbLi. The use of PbBi as an inert fluid makes the Segment Box (SB) sizing less stringent: in the case of an in-box LOCA due to a break of the water cooling circuit inside the BB SB, the pressurized volume is only the PbBi one, instead of the whole SB volume as in the reference WCLL design configuration. Consequently, the total amount of steel inside the BB can be reduced, with benefits in terms of increased tritium breeding ratio. Within this framework, University of Palermo, in support of the DCT and under the EUROfusion action, preliminarily analysed the steady-state thermal, thermo-hydraulic and normal and off-normal thermo-mechanical performances of this concept, following a theoretical-numerical approach based on finite volume and finite element methods, and adopting the ANSYS CFX and ANSYS Mechanical codes. The analyses carried out allowed a preliminary optimization of the design, improving the thermal and thermo-mechanical performances of the WCLL-db BB, in compliance with the design requirements, while reducing the total steel amount. Models, assumptions and main results are herewith reported and critically discussed.

1. Introduction

With the aim of overcoming the potential showstoppers highlighted at the end of the EU DEMO Breeding Blanket (BB) Pre-Conceptual Design phase [1,2], further BB variants have been conceived. Among them, the Water-Cooled Lead Lithium-double bundle (WCLL-db) concept was proposed at the beginning of the Conceptual Design Phase. It takes its name from the poloidally oriented db tubes, i.e. coaxial pipes with an interposed "third chamber" between them, which avoids direct contact between PbLi and water in case of in-box Loss Of Coolant Accident (LOCA). A similar solution is also adopted for the Segment Box (SB) cooling channels, where a chamber between the box and the PbLi is foreseen. These chambers are filled with an inert fluid that must be compatible with the Tokamak nuclear environment, not be chemically reacting either with water or PbLi, have a sufficiently high thermal conductivity to avoid thermal hot spots in the structures in contact with the breeder, and be characterized by a low melting point. Molten eutectic PbBi was initially selected as inert fluid. In case of an in-box LOCA, the pressurized volume is only that encompassed in between the SB and metal sheet separating the PbBi and the PbLi (namely the PbBi volume), instead of the whole SB volume as in the reference WCLL design. This allows for an easier SB sizing, reducing the total amount of steel inside the BB with benefits in terms of increased Tritium Breeding Ratio (TBR) and manufacturing, and makes it possible to easily detect in-box LOCAs by monitoring the inert fluid pressure.

In the present work, the thermofluid-dynamic and thermal–structural performances of the Left Outboard Blanket (LOB) segment of the WCLL-db concept were preliminarily investigated by means of the Computational Fluid Dynamics (CFD) code ANSYS CFX – based on the finite volume method – and of the ANSYS Mechanical code – based on the finite element method – respectively. The scope of the work was the

* Corresponding author.
E-mail address: pietroalessandro.dimaio@unipa.it (P.A. Di Maio).

https://doi.org/10.1016/j.fusengdes.2024.114335
Received 29 September 2023; Received in revised form 6 February 2024; Accepted 8 March 2024

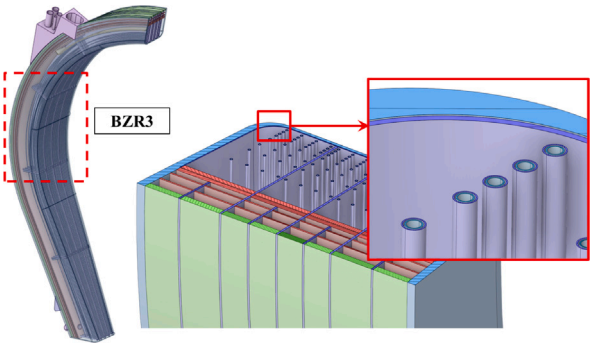

Fig. 1. WCLL-db BB LOB layout.

improvement of the design in view of the main DEMO BB requirements, also exploring the possibility of replacing the liquid PbBi with gaseous He, to solve issues related to the motion of PbBi in the thin gaps and reduce the tritium permeation. Hence, the viability of the WCLL-db BB concept has been demonstrated, in sight of a possible follow-up.

2. The geometry of the WCLL-db BB LOB segment

The reference geometric model of the WCLL-db BB LOB segment [3] is depicted in Fig. 1. It consists of a multilayer First Wall (FW) composed of a 2 mm plasma-facing surface of tungsten, an 18 mm Eurofer wall, embedded with cooling channels, a 2 mm PbBi interlayer, and a 5 mm Eurofer layer (metal sheet) devoted to separate the PbLi region from the PbBi.

The Side Walls (SWs), consisting of 41 mm of Eurofer, are thicker than the FW to compensate for the missing mechanical effect of the radial-toroidal stiffeners, not foreseen in the WCLL-db design to reduce the steel amount within the BZ, and to make the SB more robust. The rear closure is guaranteed by a 315 mm Back Supporting Structure (BSS) endowed with the cooling water manifolds, and three 12 mm-thick poloidal-radial Stiffening Plates (SPs) connect the BSS to the FW.

According to the design of [3], a liquid eutectic PbLi acting as a breeder and neutron multiplier is fed from the bottom of the segment, and it moves poloidally inside the BB. The WCLL-db BB is cooled by pressurized (155 bar) subcooled water, entering the BB at an inlet temperature of 285 °C. Water is supplied to the BB through poloidal manifolds and fed to poloidal distributors. These distributors are located at five different poloidal locations, each one identifying a different Breeder Zone Regions (BZRs). From each poloidal location, sixteen toroidally parallel-arranged distributors feed eight db tubes each (for a total of 128 tubes), responsible for Breeder Zone (BZ) cooling. Water is then collected back to an intermediate manifold located within the BSS, it is routed to the FW channels and finally collected to an outlet manifold located inside the BSS, where it leaves at a temperature of 325 °C. A schematic overview of the coolant distribution inside the BB segment with a detail of the equatorial BZR of the LOB segment, called BZR3, is shown in Fig. 2.

The present work focuses on the thermal, hydraulic, and thermo-structural study of the WCLL-db LOB BZR3.

3. Preliminary slice optimization

The preliminary study of the WCLL-db steady-state thermal performance was carried out through quasi-3D thermal simulations focussed on a thin toroidal-radial slice of the LOB BZR3 region, aimed to optimize at a reduced computational cost, the thermal field inside the component, changing the layout of the BZ db tubes.

Table 1
Bulk temperatures and heat transfer coefficients considered.

Region	T_b [°C]	h [kW/m^2 K]
Inlet manifold	285	6.6
BZ pipes	300	40.0
Intermediate manifold	315	2.5
FW channel	320	44.0
Outlet manifold	325	10.0

3.1. Quasi-3D thermal analyses setup

Starting from the geometry shown in Fig. 1, an equatorial toroidal-radial section of BZR3 was considered, obtaining the proper 2D geometry (Fig. 3).

A FW channels poloidal pitch of 13.5 mm was assumed and, consequently, the section shown in Fig. 3 was extruded of this quantity in the poloidal direction, to obtain a "quasi-3D model" hosting a single FW channel. It is placed radially 3 mm from the FW and SWs and its cross-section dimensions are equal to 7 mm × 7 mm, as per the baseline WCLL design [4].

The domain was discretized with a mesh composed of ≈3.4M nodes connected in ≈5.8M elements. Temperature-dependent properties, drawn respectively from [5–7], were assigned respectively to Eurofer, PbLi, and PbBi.

Concerning the loads and Boundary Conditions (BCs), a normal heat flux equal to 0.27 MW/m^2 was imposed on FW plasma-facing surfaces. Moreover, a purely diffusive heat transfer mode was assumed for Eurofer walls wetted by PbLi and PbBi whereas the adiabatic condition was imposed elsewhere. Regarding the volumetric density of deposited power within Eurofer, PbLi and PbBi, the spatial distributions reported in [8,9] were used as first guess values. Indeed, since the neutronic results relevant to the WCLL-db concept were not available, power density maps obtained for quite similar – yet representative – BB concepts were used. Finally, the convective heat transfer occurring between water and Eurofer was simulated considering a total mass flow rate of 122.2 kg/s circulating in the entire blanket segment [10]. In this way, using Gnielinski's correlation [11], the convective heat transfer coefficient h was calculated for each region assuming the total mass flow rate as evenly distributed among BZRs, BZ pipes and FW channels (Table 1). The latter assumption will be successively proven to be true by the results of the hydraulic analysis, discussed in Section 4.

3.2. Quasi-3D thermal analyses results

The calculated steady-state temperature distributions of the baseline configuration, depicted in Fig. 4, show that a minimum of 319 °C (above the PbLi melting temperature of 235 °C [12]) is obtained within the PbLi. Regarding Eurofer, a maximum temperature of 523 °C is predicted, below the suggested limit of 550 °C [4].

As the baseline results were compliant with the requirements, a design optimization was performed, aimed at reducing the amount of steel within the BZ, with benefits in terms of TBR, while maintaining the required thermal performances. To this purpose, four design revision iterations were carried out, as listed in the following:

- MOD1: pipes close to SPs have been moved 5.5 mm far from them, the BZ pipes have been evenly distributed considering this change and the outermost pipes have been moved towards the BSS, so to have adequate clearance between pipe manifolds and BB box corner;
- MOD2: the third row of BZ pipes has been removed and the other pipes have been rearranged to have an equal spacing between them. The h values have been updated to consider the reduced number of pipes;
- MOD3: the fifth row of pipes has been removed, rearranging the remaining rows. The h values have been revised.

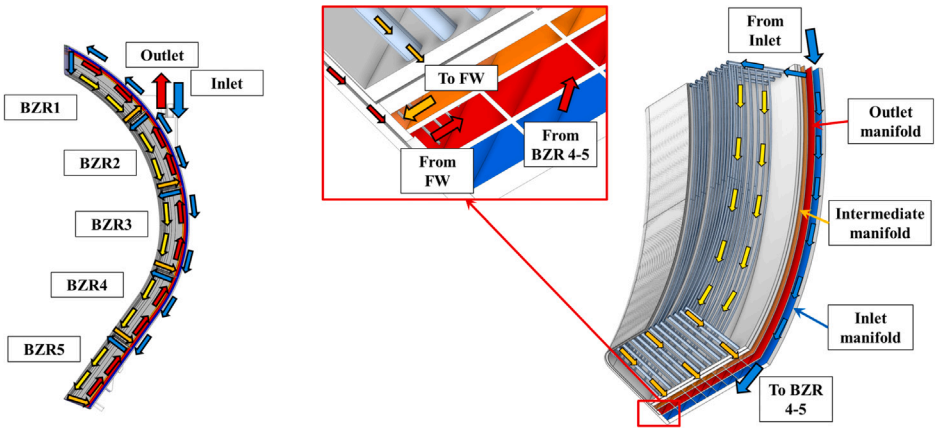

Fig. 2. Schematic overview of coolant distribution inside the WCLL-db BB LOB cooling circuit (left), and detail of the coolant flow inside the BZR3 (right).

Table 2
Maximum and minimum temperatures for the reference and the optimized layouts.

Domain	Reference	MOD1	MOD2	MOD3	MOD4
Eurofer min/max T [°C]	285/522	285/514	285/520	285/524	285/521
PbBi min/max T [°C]	307/500	308/493	308/498	308/502	308/468
PbLi min/max T [°C]	319/623	321/603	320/612	320/628	321/603

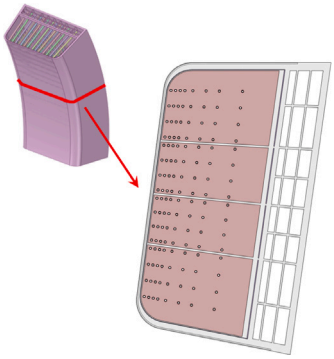

Fig. 3. Toroidal-radial slice of the WCLL-db LOB BZR3 adopted for the quasi-3D thermal analyses.

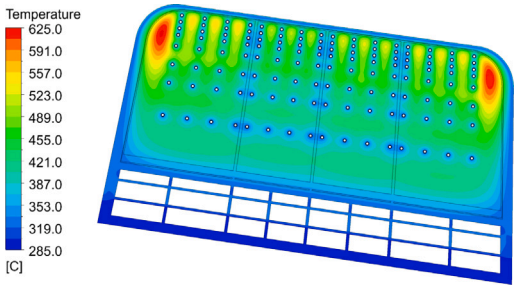

Fig. 4. Slice temperature distribution for the reference geometry.

- MOD4: the BZ pipes have been further displaced, placing the first row 3 mm far from the FW, while moving them 20 mm far from the SWs surfaces.

Results in terms of max and min temperatures are summarized in Table 2. Looking at the table, it emerges that the MOD4 layout allows quite promising thermal performances, in comparison with the reference configurations, with a 25% reduction in the number of BZ pipes. The thermal field obtained with the MOD4 configuration is shown in Fig. 5.

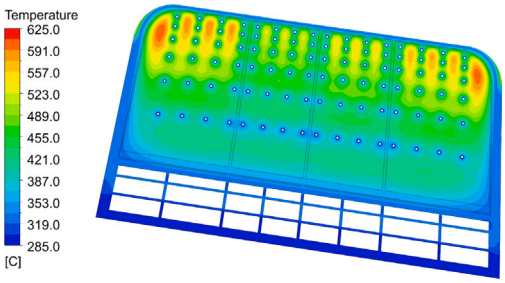

Fig. 5. Slice temperature distribution for the MOD4 geometry.

It is moreover worth mentioning that increasing the bulk temperature of the BZ pipes coolant from 300 to 315 °C, so to reproduce a configuration representing a slice of the BZR very close to the collectors of the BZ pipes, the maximum Eurofer temperature is increased by less than 2.5 °C. This occurs because the maximum temperature in the Eurofer is observed at the metal sheet of the SB corner, where the temperatures in the structures are mainly affected by the FW coolant temperature.

4. CFD analysis of the WCLL-db LOB BZR3 cooling circuit

In this section, a 3D steady-state fluid-dynamic analysis of the WCLL-db LOB BZR3 cooling circuit, carried out with an isothermal CFD calculation, is presented. The MOD4 layout was adopted for BZ pipes. The analysis was performed to assess the cooling circuit's hydraulic performances in terms of the coolant's pressure drop and mass flow rate distribution.

4.1. CFD analysis setup

The steady-state hydraulic performances of the WCLL-db LOB BZR3 cooling circuit were assessed considering the assumptions, loads, and BCs reported in Table 3.

In order to speed up the analysis, the water inlet manifold was not modelled, selecting the sixteen radial distributors of the BZ pipes as the domain inlets. In addition, it was assumed that the intermediate

Table 3
Summary of the hydraulic analysis setup.

Analysis type	Steady-state isothermal
Material library	Water IAPWS IF97 [13]
Ave. Fluid temperature	305 °C
Turbulence model	k-ω SST
Near-wall treatment	Automatic wall functions (High Reynolds formulation)
Inlet manifold (inlet) BC	155 bar total pressure
Outlet manifold BC (inlet from lower BZRs)	48.88 kg/s
Outlet manifold BC (outlet to upper BZRs)	73.32 kg/s
Wall BCs	No-slip condition surface roughness of 15 μm

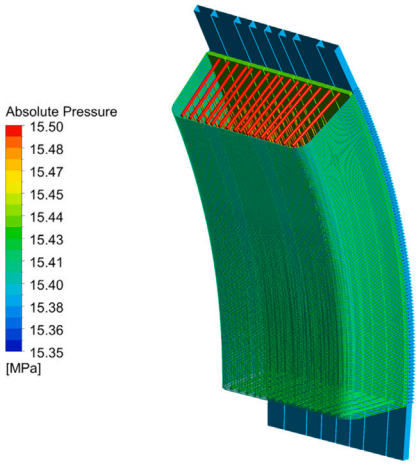

Fig. 6. WCLL-db LOB BZR3 coolant pressure field.

manifolds are closed at the top and bottom ends of the BZR3, in order to simplify the assignment of BCs.

The mesh parameters were assigned starting from a preliminary validation campaign, not reported here for the sake of brevity. In particular, the attention was focused on a single FW channel and one BZ cooling pipe, comparing the results in terms of pressure drop with correlations available in literature. The validation campaign allowed establishing that employing ≈42k elements for a single FW channel and ≈80k elements for a BZ pipe is sufficient to obtain a good accuracy of the results. Starting from these findings, a mesh composed of ≈29.8M nodes and ≈43.9M elements was generated for the entire BZR3 cooling circuit.

4.2. CFD analysis results

The coolant pressure spatial distribution within the WCLL-db LOB BZR3 cooling circuit is shown in Fig. 6. It is interesting to note that the entire WCLL-db LOB BZR3 cooling circuit is characterized by a modest total pressure drop, equal to 1.16 bar. Approximately 52% of it is related to the BZ pipes and their distributors (0.64 bar), while the remaining 48% is related to the FW channels (0.52 bar). The contribution to the overall pressure drop of the outlet and intermediate manifold is negligible since pressure drop values in the order of a few hundred Pascals are predicted by the simulation.

The mass flow rate distribution among the FW channels is depicted in Fig. 7, where the numbering of the channel goes from bottom to top, showing an even distribution, characterized by an average value of 0.116 kg/s and a relative standard deviation of 0.38%. Similar results are obtained also for the BZ cooling pipes, as visible Fig. 8 together with an indication of the cooling pipes numbering. The distribution is

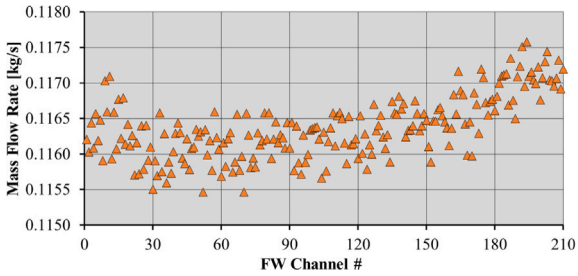

Fig. 7. Mass flow rate distribution among FW channels.

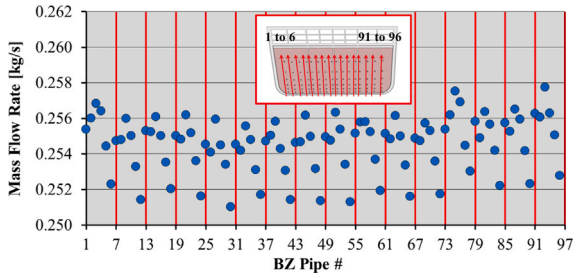

Fig. 8. Mass flow rate distribution among BZ channels.

characterized by an average value of 0.255 kg/s and a relative standard deviation of 0.61%.

The reported flow distributions clearly confirm that the assumption of uniform flow distribution in the FW channels and the BZ pipes adopted for the quasi-3D thermal analyses of Section 3 is valid. Hence one can conclude that the MOD4 layout shows promising thermal and hydraulic behaviour and, then, it can be further assessed from the structural point of view.

5. The thermal–structural assessment

A campaign of steady-state thermo-mechanical analyses was carried out considering the Normal Operation (NO) and Over-Pressurization (OP) (namely the loading conditions relevant to the in-box LOCA event) steady-state loading scenarios. Results were assessed in view of the RCC-MRx structural design criteria [14]. At first, preliminary thermo-mechanical analyses of the same slice used for the thermal analyses described in Section 3 were performed, focussing on the design of suitable poloidal-radial ribs connecting the metal sheet with the SB and the BSS, to guarantee the structural integrity of the system under NO and OP conditions.

The results of these analyses, not reported for the sake of brevity, showed an unsatisfactory thermo-mechanical performance, due to unacceptable deformations of the metal sheet under OP conditions. Hence, in response to the difficulties arising in the use of poloidal-radial ribs, a different concept was studied, using alternatively toroidal-radial ribs, thus requiring a fully-3D model.

A campaign to determine whether this revised concept can withstand the OP loads was therefore performed, exploring different toroidal-radial rib configurations. In particular, three geometrical quantities were assumed as parameters for this study: the thickness of the metal sheet (s_1), the thickness of the toroidal-radial ribs (s_2), and the number of FW channels in between two toroidal-radial ribs (N), as shown in Fig. 9. Globally, 27 cases were considered (Table 4) to be assessed under NO and OP loading scenarios.

To reduce the computational time required to perform the study, dedicated screening thermal analyses were carried out, evaluating the maximum Eurofer temperature so to preliminary discard all those cases in which temperatures higher than 550 °C were predicted.

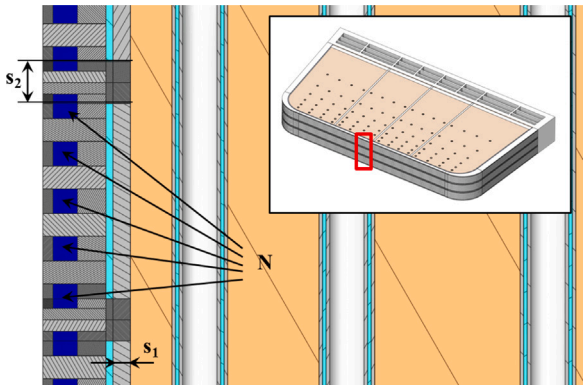

Fig. 9. Detail of the selected geometrical parameters.

Table 4
Maximum Eurofer temperatures for all the cases investigated.

#	N [–]	s_1 [mm]	s_2 [mm]	T_{max} [°C]
RUN01	3	5	10	537.96
RUN02	3	7.5	10	546.63
RUN03	3	10	10	553.88
RUN04	3	5	12	536.87
RUN05	3	7.5	12	545.95
RUN06	3	10	12	553.11
RUN07	3	5	14	536.26
RUN08	3	7.5	14	545.22
RUN09	3	10	14	552.21
RUN10	5	5	10	538.79
RUN11	5	7.5	10	547.75
RUN12	5	10	10	555.47
RUN13	5	5	12	538.71
RUN14	5	7.5	12	547.02
RUN15	5	10	12	555.19
RUN16	5	5	14	538.29
RUN17	5	7.5	14	546.96
RUN18	5	10	14	554.78
RUN19	7	5	10	552.06
RUN20	7	7.5	10	560.23
RUN21	7	10	10	567.31
RUN22	7	5	12	551.59
RUN23	7	7.5	12	559.31
RUN24	7	10	12	566.64
RUN25	7	5	14	551.26
RUN26	7	7.5	14	559.70
RUN27	7	10	14	566.84

5.1. Screening thermal analyses

The screening thermal analyses were performed on a 3D toroidal-radial slice of the WCLL-db LOB BZR3 region, considering the same thermal loads and BCs already discussed in Section 3.1, except for the volumetric density of deposited nuclear power that was drawn from neutronic analysis relevant to the WCLL-db LOB [15].

The results obtained for the 27 geometrical configurations investigated are summarized in Table 4, where the discarded configurations, characterized by Eurofer temperatures higher than 550 °C, are highlighted in red.

As it can be argued, the maximum Eurofer temperature increases for increasing s_1 and N values, and it decreases for higher s_2 values. It is worth noting that, for all the considered configurations, the maximum temperature is always located in the metal sheet at the BB corner, as depicted in Fig. 10. As for the thermal analyses of Section 3, an increase of the BZ coolant temperature from 300 to 315 °C does not significantly affect the maximum temperature in Eurofer, with deviations of ≈2 °C.

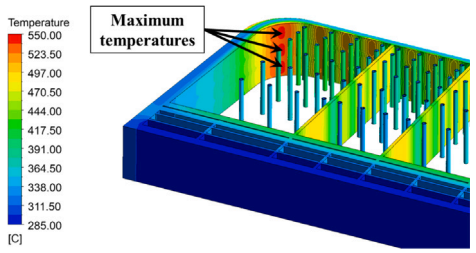

Fig. 10. Maximum temperature location in Eurofer.

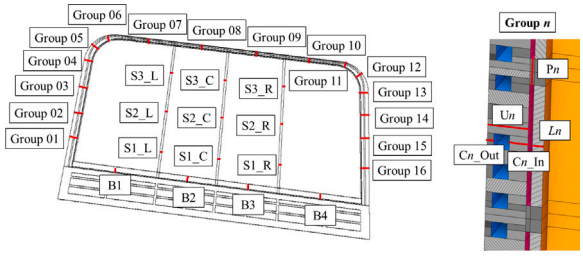

Fig. 11. Location of the groups of paths (a) and individual paths of each group (b).

5.2. Thermo-mechanical parametric analyses

Once the screening thermal analyses were completed, the 12 surviving configurations (Table 4) were assessed from the structural standpoint, in compliance with the RCC-MRx structural design code.

5.2.1. Thermo-mechanical parametric analyses setup

The computational domain was selected considering a poloidal extension such that $3N$ cooling channels are hosted. The domain was discretized with a mixed tetra-hexa mesh grid with a target length of 5 mm, resulting in meshes ranging from ≈1.5M nodes connected in ≈1.0M elements for the cases with $N = 3$ to ≈2.0M nodes connected in ≈1.5M elements for the cases with $N = 5$.

The temperature-dependent Eurofer thermo-physical and mechanical properties were assigned [5], and the relevant temperature field was imported from the results of Section 5.1.

Moreover, the loads and boundary conditions characterizing the NO and OP scenarios [16] were considered. In particular, as to the pressure load to be applied in both scenarios, the water design pressure of 17.85 MPa was imposed on all water-cooled surfaces and a hydrostatic pressure value of 2.0 MPa was assumed for PbLi [17]. Concerning the PbBi, it was supposed a hydrostatic pressure of 1.0 MPa in NO, whereas a pressure of 17.85 MPa was assigned in OP.

Lastly, as to the mechanical constraints, the typical set of radial, toroidal and poloidal boundary conditions largely adopted for the structural analysis of the WCLL slices was introduced [18,19], including a realistic generalized plane strain condition in the upper slice faces [20].

5.2.2. Thermo-mechanical parametric analyses results

To evaluate the thermo-mechanical performance of the WCLL-db SB design, a stress linearization procedure was performed along 93 paths located within the most critical regions of the structure (Fig. 11).

Then, the fulfilment of Level A and D criteria prescribed by the RCC-MRx design code, for the NO and OP loading scenario respectively, was checked by adopting an automated procedure based on ANSYS Mechanical scripting.

Out of the 93 paths considered, only 23 presented criticalities for at least one of the configurations analysed. Seven of these paths were common among all configurations and were not related to the

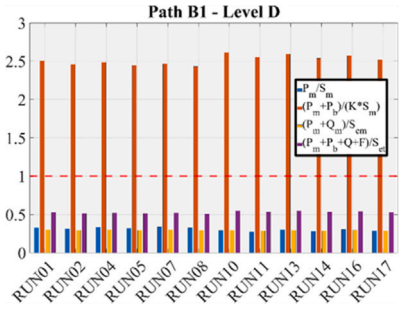

Fig. 12. Stress linearization results under OP for path B1.

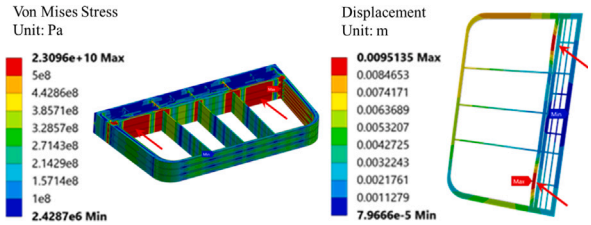

Fig. 13. Critical BSS metal sheet regions.

design of the toroidal-radial ribs. The most promising rib configuration among those examined is the RUN11 (N = 5, s_1 = 7.5 mm and s_2 = 10 mm), being the one with the lowest number of critical paths. The following sections focus on the results of this configuration, for which only the seven common paths were not compliant with at least one criterion, giving a brief overview of the outcomes obtained for the other investigated rib configurations.

Normal operation scenario

Under NO conditions, five critical paths are observed for RUN11. Three of them are located inside the SPs (close to the BSS) and two are in the outer part of the FW, i.e. C7_Out and C10_Out, even though the criteria are exceeded by less than 20%. As to the critical paths within the SPs, they are failing because of secondary stress, and an adjustment of the BZ tube's spatial distribution could help in reducing the temperature in SPs, leading to an improvement of their structural performances.

To summarize the results of the other toroidal-radial ribs' geometrical configurations, it is worth mentioning that among the paths located within the metal sheet and their ribs, only paths L6 and P6 present some criticalities. The failure is due to the high temperature along the paths, which are located in the zone of maximum temperature in Fig. 10, with consequent low values for the stress limits. Regarding the paths located in the FW and SW in between two FW channels (Un), those located between the FW channels and the PbBi interlayer (Cn_In), and the paths within the BSS metal sheet, no issues are encountered.

As most of the criticalities are related to secondary stresses, a slight re-arrangement of the BZ tubes could improve the temperature distribution, thus enabling the adoption of other rib configurations.

Over-pressurization scenario

Under OP conditions, RUN11 presents criticalities (with criteria > 1.2) only in the paths located within the BSS metal sheet, i.e. B1 and B4. The failure of the criteria in these paths is caused by primary loads, as reported in Fig. 12 as a matter of example. This is due to the absence of a mechanical connection between the BSS and the metal sheet, as visible in Fig. 13, where it is also possible to observe deformations of magnitude lower than 10 mm in the structure. This issue can be easily solved by adopting proper ribs connecting the metal sheet to the BSS.

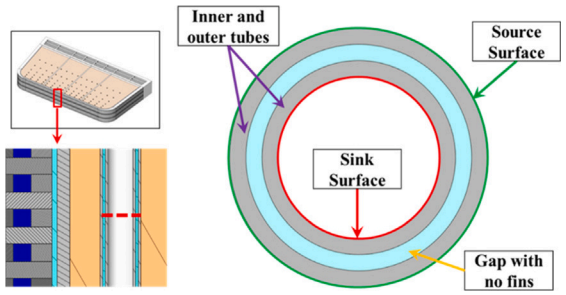

Fig. 14. Geometry and nomenclature adopted for the db tubes.

Regarding the other rib geometrical configurations analysed, all the paths located within the metal sheet for the cases with N = 5 and s_1 = 5 mm fail due to primary load, while no other issues are encountered elsewhere.

The results of this exploratory study are encouraging, as most of the criticalities encountered can be easily solved. Moreover, for future follow-ups of this activity, it could be investigated the possibility of reducing the thickness of the toroidal-radial ribs s_2, since no significant criticalities related to their structural performances are found, and the possibility of selecting a metal sheet thickness s_1 in between 5 and 7.5 mm, increasing the breeder inventory.

6. Thermal analyses of a breeder zone region of the WCLL-db with gas gap and fins

Following the promising results described in Section 5.2.2, the possibility of replacing the PbBi with helium was considered so as to avoid the filling issues expected by adopting this liquid metal and to remove the tritium produced in the BZR before it reaches the coolant. A drawback is represented by the significant difference in the thermal conductivity of the two materials: that of PbBi is equal to 13.12 W/m K at 400 °C [7] whereas the helium one amounts to 0.27 W/m K at the same temperature [21]. Consequently, the temperature difference across the gap would be increased by a factor of ≈50. It is therefore clear that maintaining the same system design would result in excessive temperatures in the breeder and in the Eurofer of the db tube and the metal sheet. A potential solution to guarantee a comparable thermal performance between the gap filled with PbBi and the one with helium, without selecting unduly thin gaps, is to resort to finned structures, with fins connecting the components between which the gap is interposed. As a thermal parametric analysis campaign of a complete slice equipped with finned tubes and sheet is computationally too expensive, this solution was investigated by performing detailed thermal analyses of the single finned elements, comparing their thermal performance with those of the same components of the reference geometry, having the gap filled with PbBi.

In particular, a three-step procedure was followed, composed of: a parametric study of the steady-state thermal performance of a 2D section of a db tube equipped with fins; a parametric study of the steady-state thermal performance of a 2D section of the metal sheet equipped with fins; a parametric study of the steady-state thermal performance of the best configurations resulting from the former parametric analyses.

6.1. Parametric 2D analysis of a db tube

The parametric 2D analysis of a db tube with helium-filled gaps and fins focused on the geometry depicted in Fig. 14, where the "source surface" is in contact with the breeder, so characterized by the higher temperatures, while the "sink surface" is in contact with the coolant.

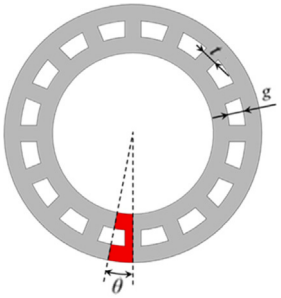

Fig. 15. Considered db tube sector (in red) and relevant parameters (t and g) for a configuration with $N = 16$.

6.1.1. Parametric 2D analysis of a db tube setup

The imposed BCs consist of heat flux at the source surface equal to 1 MW/m^2, and convection at the sink surface (58 kW/m^2 K and 300 °C). No volumetric heat loads were taken into account and the thermal conductivities of the different materials were considered to be temperature-dependent, adopting the data and relevant correlations drawn from [5,7,21]. The thermal performance comparison is based on a single indicator, namely the overall Heat Transfer Coefficient (HTC), whose definition is given in Eq. (1), where q'' is the imposed heat flux, while $\overline{T}_{source}$ and $\overline{T}_{sink}$ are respectively the surface-averaged temperature on the source and sink surfaces. For the db tubes, the heat flux is calculated at the source surface.

$$HTC = \frac{q''}{(\overline{T}_{source} - \overline{T}_{sink})} \tag{1}$$

A total of 23 different geometrical configurations was investigated, obtained by changing the number of fins (N) ranging from 2 to 16, considering two values of thickness (t), namely 1 and 2 mm, and two values of the thickness of the gap (g), namely 1 and 0.5 mm. The thickness of the inner and the outer tubes was considered unchanged with respect to the reference design. Due to the symmetry of the problem, only a small sector of the pipe was considered, shown in red in Fig. 15 together with the parameters considered for the parametric analysis.

The number of fins N was changed simply by acting on the angular extension θ of the domain, which can be easily related to N by the formula given in Eq. (2).

$$\theta = \frac{360°}{2N} \tag{2}$$

To simplify the automatic creation of the geometry, helium was neglected, and the gap surfaces were simulated with an adiabatic BC. The results thus obtained are conservative, as the actual HTC values will be slightly higher, as part of the heat transfer will take place within the helium thickness. In detail, dedicated analyses showed how the underestimation of HTC ranges from ≈10%, for the configurations characterized by a few fins, to less than 3% considering a high number of fins.

6.1.2. Parametric 2D analysis of a db tube results

The outcomes of the parametric analyses are summarized in Fig. 16, showing a comparison with 5.60 kW/m^2 K, the HTC for the db tube with the PbBi-filled gap, preliminarily calculated through a dedicated 2D numerical simulation of the db tube under the same BCs adopted for the parametric analyses. The temperature field of one of the configurations is reported instead in Fig. 17.

As can be argued, HTC values comparable to or even higher than those obtained for the PbBi configuration can be obtained by using low g values (0.5 mm), a high number of fins and a high t-thickness, which is not surprising as these features result in a high volumetric fraction of Eurofer, characterized by a higher thermal conductivity than PbBi.

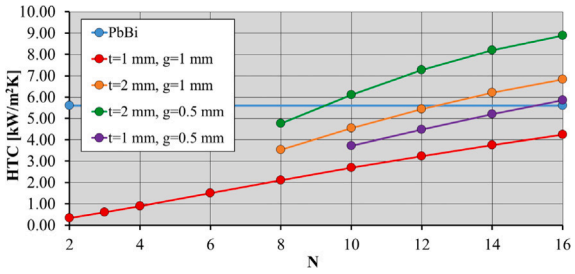

Fig. 16. Outcomes of the parametric thermal analyses of the db tubes equipped with fins.

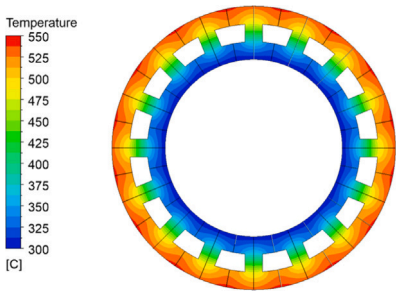

Fig. 17. Resulting thermal field for the configuration $t = 1$ mm, $g = 1$ mm, $N = 16$.

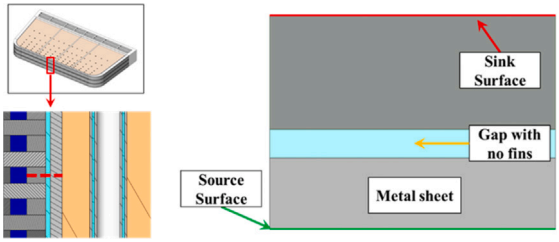

Fig. 18. Geometry and nomenclature adopted for the metal sheet.

6.2. Parametric 2D analysis of the metal sheet

The parametric 2D analysis of the metal sheet with helium-filled gaps and fins focused on the geometry depicted in Fig. 18.

6.2.1. Parametric 2D analysis of the metal sheet setup

The imposed BCs consist of heat flux at the source surface equal to 0.5 MW/m^2, and convection at the sink surface (44 kW/m^2 K and 320 °C), while no volumetric heat loads and material properties already employed in Section 6.1 were considered. The parametric analysis was performed considering two values of t, namely 1 and 2 mm, three values of g, namely 2, 1, and 0.5 mm, and different values of fin density n, defined as the number of fins per unit length of the metal sheet, ranging from 100 to 500 fin/m, for a total of 48 simulations. Due to the symmetry of the problem, only a small region of the metal sheet and SB domain was considered, shown in red in Fig. 19, together with the parameters considered for the parametric analysis.

The fin density n was changed simply by acting on the value l, which can be easily related to n by Eq. (3).

$$l = \frac{1}{2n} - \frac{t}{2}. \tag{3}$$

6.2.2. Parametric 2D analysis of the metal sheet results

In order to have a reference value, the HTC for the metal sheet with the PbBi-filled gap was preliminarily calculated, resulting equal

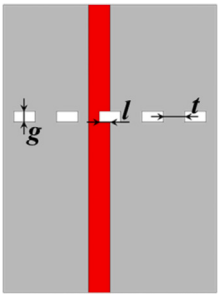

Fig. 19. Considered metal sheet and segment box domain (in red) and relevant parameters.

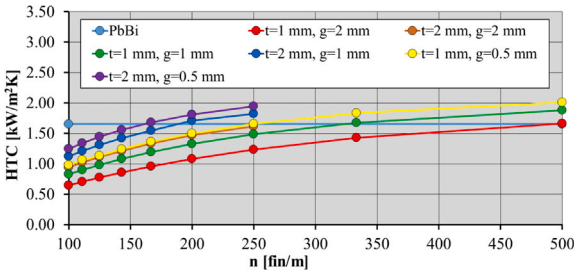

Fig. 20. Outcomes of the parametric thermal analyses of the metal sheet equipped with fins.

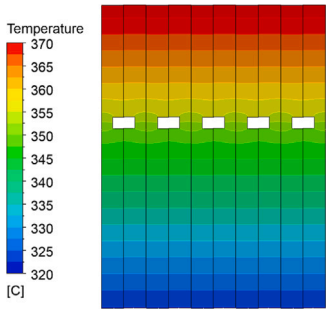

Fig. 21. Resulting thermal field for the configuration t = 1 mm, g = 0.5 mm, 500 fin/m.

to 1.65 kW/m^2 K. The outcomes of the parametric analyses are summarized in Fig. 20, while the details of the thermal field for one of the configurations are depicted in Fig. 21.

As for the db tubes, HTC values comparable to or even higher than those obtained for the PbBi configuration can be obtained by using low g values (1, 0.5 mm), a high number of fins per unit length and a high t-thickness. Regarding the fin density values chosen for the analyses, it should be pointed out that maximum values of 250 and 500 fin/m were chosen depending on the thickness t of the fins, to have at most a ratio of 0.5 between the fin contact surface (metal sheet-SB) and the total metal sheet surface.

6.3. Parametric analysis on the influence of contact thermal resistance of db tubes and metal sheet

The parametric study of the thermal performance of the best geometric configurations of the db tubes and the metal sheet was carried out with the twofold aim of assessing the effects of thermal contact efficiency on the overall thermal behaviour, and of determining the reduction in HTC if a thin gap between the two parts is purposely foreseen, acting as a tritium transport barrier.

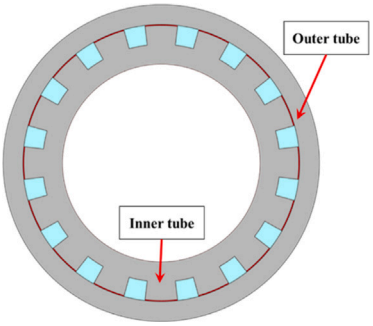

Fig. 22. Location of the thermal contact resistance (in red) for a db tube. The helium region is shown in light blue.

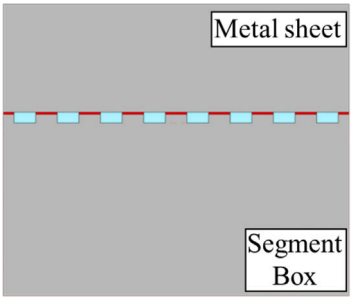

Fig. 23. Location of the thermal contact resistance (in red) for the metal sheet. The helium region is shown in light blue.

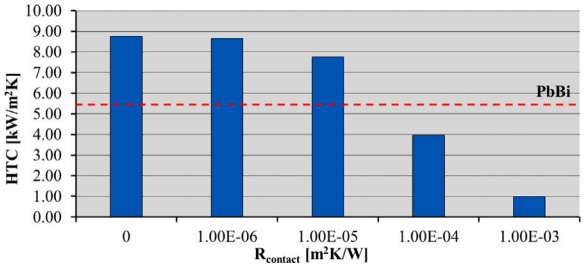

Fig. 24. Overall db tube HTC variation with the thermal contact resistance.

6.3.1. Parametric analysis on the influence of contact thermal resistance setup

The parametric analysis was carried out considering the presence of helium, to avoid unduly underestimations of the overall HTC values, in particular for those configurations characterized by high thermal contact resistances. Convective phenomena within the helium were however neglected and only thermal conduction was taken into account. The thermal contact resistance location is shown in red in Fig. 22 for the db tubes, and in Fig. 23 for the metal sheet.

The analyses were performed by varying the thermal contact resistance from 0 to 10^{-3} m^2 K/W.

6.3.2. Parametric analysis on the influence of contact thermal resistance results

Concerning the db tubes, parametric thermal steady-state analyses were carried out for three different geometric configurations, but only the most promising results – namely those of the geometry characterized by N = 16, t = 2 mm, g = 0.5 mm – are shown in Figs. 24 and 25 for the sake of brevity.

Regarding the metal sheet, a single parametric steady-state thermal analysis campaign was carried out for the geometrical configuration

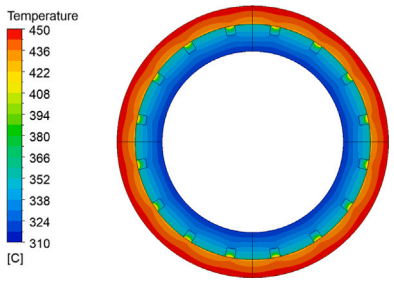

Fig. 25. Temperature distribution on the db tube for a contact thermal resistance of 10^{-4} m^2 K/W.

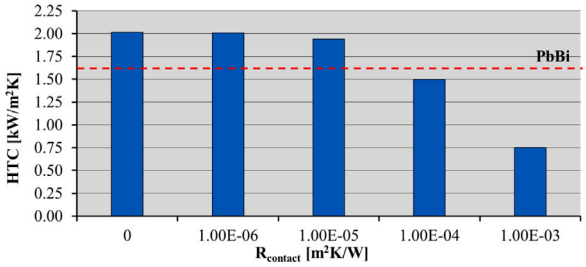

Fig. 26. Overall metal sheet HTC variation with the thermal contact resistance.

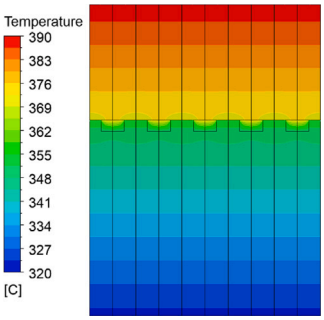

Fig. 27. Temperature distribution on the metal sheet for a contact thermal resistance of 10^{-4} m^2 K/W.

characterized by n = 500 fin/m, t = 1 mm and g = 0.5 mm, the results of which are illustrated in Figs. 26 and 27.

It can be noticed that, both for the db tube and the metal sheet, thermal contact resistance values higher than 10^{-4} m^2 K/W lead to HTC values significantly lower than the relevant reference cases (with PbBi) even for the configuration with the higher thermal performance. Furthermore, the presented results can be employed to provide an estimation of the overall HTC obtained when a small helium thickness is interposed between the components, aiming to reduce the tritium permeation to the coolant. In particular, given a defined thickness of this thin helium gap δ, it is possible to calculate the corresponding contact thermal resistance through

Eq. (4):

$$R_{contact} = \frac{\delta}{\lambda}. \quad (4)$$

By adopting this thermal contact resistance is thus possible to interpolate the data provided in the figures above to obtain a rough estimation of the overall HTC value both for the db tube and the metal sheet.

7. Conclusion

The thermofluid-dynamic and thermal–structural assessment of the WCLL-db BB concept has been presented in this paper. The obtained results have allowed achieving a viable geometric layout for the equatorial region of the LOB segment, paving the way for future and more detailed design analysis. At the same time, a variant encompassing helium instead of liquid PbBi within the "double bundle" chambers has been developed, providing a design solution to overcome the main issues in terms of liquid metal management and tritium permeation posed by the nature of this concept. Starting from the outcomes presented in this paper, a dedicated campaign of analysis can be launched to attain a robust conceptual design for the WCLL-db BB concept, capable of fully matching the prescribed DEMO design requirements.

CRediT authorship contribution statement

P.A. Di Maio: Conceptualization, Investigation, Methodology, Writing – original draft. **I. Catanzaro:** Conceptualization, Investigation, Methodology, Writing – original draft. **G. Bongiovì:** Conceptualization, Investigation, Methodology, Writing – original draft. **F.M. Castrovinci:** Conceptualization, Investigation, Methodology, Writing – original draft. **P. Chiovaro:** Conceptualization, Investigation, Methodology, Writing – original draft. **S. Giambrone:** Conceptualization, Investigation, Methodology, Writing – original draft. **A. Gioè:** Conceptualization, Investigation, Methodology, Writing – original draft. **F.A. Hernández:** Conceptualization, Investigation, Methodology, Writing – original draft. **I. Moscato:** Conceptualization, Investigation, Methodology, Writing – original draft. **G.A. Spagnuolo:** Conceptualization, Investigation, Methodology, Writing – original draft. **A. Quartararo:** Conceptualization, Investigation, Methodology, Writing – original draft. **E. Vallone:** Conceptualization, Investigation, Methodology, Writing – original draft.

Declaration of competing interest

The authors declare that they have no known competing financial interests or personal relationships that could have appeared to influence the work reported in this paper.

Data availability

Data will be made available on request.

Acknowledgements

This work has been carried out within the framework of the EUROfusion Consortium, funded by the European Union via the Euratom Research and Training Programme (Grant Agreement No 101052200 — EUROfusion). Views and opinions expressed are however those of the author(s) only and do not necessarily reflect those of the European Union or the European Commission. Neither the European Union nor the European Commission can be held responsible for them.

References

[1] T. Donné, W. Morris, European Research Roadmap to the Realisation of Fusion Energy, ISBN: 978-3-00-061152-0, 2018.
[2] L.V. Boccaccini, et al., Status of maturation of critical technologies and systems design: Breeding blanket, Fusion Eng. Des. 179 (2022) 113116, http://dx.doi.org/10.1016/j.fusengdes.2022.113116.
[3] F. Hernández, WCLL-db LOBS, 2021, EUROfusion IDM Ref.: 2P5S3J v1.0.
[4] A. Del Nevo, P. Arena, Internal deliverable BB-3.2.1-T007-D001: WCLL BB design and integration studies 2020 activities, 2020, EUROfusion IDM Ref.: 2NTP7J v1.1.
[5] E. Gaganidze, DEMO-DEF-1-CD1 - Materials properties handbook - EUROFER97, 2023, EUROfusion IDM Ref.: 2NZHBS v1.3.
[6] D. Martelli, A. Venturini, M. Utili, Literature review of lead-lithium thermophysical properties, Fusion Eng. Des. 138 (2019) 183–195.
[7] OECD, N.E. Agency, Handbook on lead-bismuth eutectic alloy and lead properties, materials compatibility, thermalhydraulics and technologies, 2015, p. 950.

[8] A. Del Nevo, M. Oron-Carl, P. Arena, Internal deliverable BB-3.2.1-T006-D001: WCLL BB design and integration studies 2019 activities, 2020, EUROfusion IDM Ref.: 2P5NE5 v1.0.
[9] G. Zhou, M. Oron-Carl, Internal deliverable BB-1.2.1-T005-D005: Design studies on alternative solid breeder blanket configurations in 2018, 2019, EUROfusion IDM Ref.: 2P5CF4 v1.0.
[10] F. Hernández, I. Moscato, G. Spagnuolo, M2-1 PSDD-Task_WCLL-db_1st_Progress_Meeting, 2021, EUROfusion IDM Ref.: 2NT8K8 v1.0.
[11] T. Bergman, A. Lavine, F. Incropera, Fundamentals of Heat and Mass Transfer, seventh ed., John Wiley & Sons, Incorporated, 2011.
[12] G. Bongiovì, F. Franza, I. Maione, BB.WCLL-DEF-2-CD1-BB WCLL SRD, 2020, EUROfusion IDM Ref.: 2P3HGL v1.6.
[13] International Association for the Properties of Water and Steam, Revised release on the IAPWS industrial formulation 1997 for the thermodynamic properties of water and steam, 2007.
[14] AFCEN, RCC-MRx, design and construction rules for mechanical components of nuclear installations, 2013.
[15] P. Pereslavtsev, et al., Neutronic activity for development of the promising alternative water-cooled DEMO concepts, Appl. Sci. 13 (13) (2023) http://dx.doi.org/10.3390/app13137383.
[16] G. Spagnuolo, et al., Development of load specifications for the design of the breeding blanket system, Fusion Eng. Des. 157 (2020) 111657, http://dx.doi.org/10.1016/j.fusengdes.2020.111657.
[17] R. Mozzillo, WCLL LiPb loops in 2020 configuration, 2021, EUROfusion IDM Ref.: 2NYDZQ.
[18] P.A. Di Maio, et al., On the effect of stiffening plates configuration on the DEMO Water Cooled Lithium Lead Breeding Blanket module thermo-mechanical behaviour, Fusion Eng. Des. 146 (2019) 2247–2250, http://dx.doi.org/10.1016/j.fusengdes.2019.03.163.
[19] P.A. Di Maio, et al., Analysis of the thermo-mechanical behaviour of the DEMO Water-Cooled Lithium Lead breeding blanket module under normal operation steady state conditions, Fusion Eng. Des. 98–99 (2015) 1737–1740, http://dx.doi.org/10.1016/j.fusengdes.2015.03.051.
[20] G.A. Spagnuolo, Integrated Multi-Physics Design Tool for Fusion Breeding Blanket Systems - Development and Validation (Ph.D. Thesis), 2020.
[21] P.J. Linstrom, NIST chemistry webbook, NIST standard reference database number 69, http://dx.doi.org/10.18434/T4D303.